2D-DNS OF QUASI-2D TURBULENCE IN SHALLOW WATER

ROB UITTENBOGAARD, BAS VAN VOSSEN
J.M. Burgers Centre, Delft University of Technology, The Netherlands
WL|Delft Hydraulics, The Netherlands

Abstract

Through a series of cases, we investigate the possibilities of the shallow-water solver Delft3D-Flow of simulating the evolution of (quasi-)2D turbulence in shallow water subjected to internal and external friction and forcing.
This paper presents the simplest case, namely the 2D-DNS of laboratory experiments of freely-evolving 2D turbulence, initiated by a rake in a shallow fresh-water layer on top of a salt-water layer in a square 1*1 m^2 basin (Maassen 2000). Tabeling et al. (1991) report similar experiments in a fluid with a free surface but initiated by vortices counter-rotating in a chessboard arrangement.
Likewise, our depth-averaged free-surface simulations are initiated by random as well as by chessboard vortices. We compare the temporal evolution of the simulated vorticity field in a viscous fluid with observations as well as with simulations of Clercx et al. (1999) dedicated to incompressible 2D turbulence simulation with a rigid lid. Theirs and our simulations agree with the experimentally observed evolution of vorticity into just two vortices with opposite rotation. All simulations neglect the friction at the density interface and exhibit lesser decay of kinetic energy than observed in the experiments of Maassen (2000).

1. Introduction

Based on the hydrostatic-pressure assumption, the shallow-water solver Delft3D-Flow has been extensively used for modeling the depth-averaged or 3D flows in civil-engineering applications.
For better assessment of ship traffic, structural stability, sediment transport, dredging operations and algae blooms, there appears to be a growing interest in simulating more details of the flow such as the temporal and spatial pdpf's of horizontal velocity, bed-shear stress, mixtures of dissolved or suspended constituents etc.
Rather than developing 2D turbulence closures, we prefer resolving and simulating most of the horizontal flow patterns. Although, practical feasibility demands that we maintain modeling the 3D turbulence in the orthodox manner using partial-slip, bed friction and 3D turbulence closures for boundary-layer

type of flows. We define the latter approach as Horizontal Large Eddy Simulation (HLES) acknowledging the particular properties of shallow-water flows. Recently, this HLES approach has been validated against observations of a shallow-water mixing layer (Kernkamp & Uittenbogaard, 2001).
The essential question is whether the available general-purpose shallow-water solver is suitable for HLES, particularly, its numerical dissipation and the accuracy constraints for simulating 2D-turbulence in free-surface flows. This paper deals with these fundamental questions by simulating laboratory experiments of 2D turbulence freely-evolving in a square basin.

2. The shallow-water solver Delft3D-Flow

In depth-averaged mode, Delft3D-Flow solves the following depth-averaged shallow-water equations (SWE) for mass conservation and for the depth-averaged horizontal velocity:

$$\frac{\partial \zeta}{\partial t} + \nabla \cdot (h\underline{u}) = 0 \text{and} \frac{\partial \underline{u}}{\partial t} + \underline{u} \cdot \nabla \underline{u} + g\nabla\zeta = \nu\nabla^2 \underline{u} + \underline{T} - h^{-1} c_f |\underline{u}|\underline{u}. \tag{1}$$

In (1), $\underline{u}$=(u,v) is the depth-averaged horizontal velocity vector, $h=d+\zeta$ the total depth, d the still-water depth and ζ the free-surface position, both referring to some horizontal reference plane, c_f the bed-friction coefficient, ν the kinematic viscosity and g the magnitude of gravitational acceleration. The bed friction term is the depth average of the force by the Reynolds-shear stress of 3D turbulence without wind. The force vector $\underline{T}$ is due to subgrid-scale stresses. Bed friction and $\underline{T}$ are omitted in this paper but applied by Kernkamp & Uittenbogaard (2001) for simulating a shallow-water mixing layer. The term $g\nabla\zeta$ represents the horizontal gradient of pressure based on the hydrostatic-pressure assumption. On a staggered (Arakawa-C) grid, the horizontal terms in (1) are formulated in curvilinear orthogonal co-ordinates but in this paper we consider just Cartesian (x,y)-(u,v) grids.
The SWE (1) are time integrated by ADI of which the first half time step, from t=nΔt to (n+½)Δt, begins by solving the discretised v-momentum equation:

$$\frac{v^{n+\frac{1}{2}} - v^n}{\frac{1}{2}\Delta t} + u^n D_x^{2^{nd}\,upw}\left\{v^{n+\frac{1}{2}}\right\} + v^n D_y^{2^{nd}\,upw}\left\{v^{n+\frac{1}{2}}\right\} + gD_y^{2^{nd}\,cntrl}\left\{\zeta^n\right\} = 2\nu D_x^{2^{nd}\,cntrl}\left\{D_x^{2^{nd}\,cntrl}\left\{v^n\right\}\right\} + 2\nu D_y^{2^{nd}\,cntrl}\left\{D_y^{2^{nd}\,cntrl}\left\{v^n\right\}\right\} \tag{2}$$

where D_α is a first-order difference operator with respect to a horizontal Cartesian co-ordinate α=x,y. For the advection terms in (2), D_α is 2nd order

upwind but 2nd order central for pressure as well as stresses. Eq. (2) is implicit for $v^{n+½}$, solved by red-black Jacobi while pressure and twice the Laplacian $\nu\nabla^2 v$ are integrated explicitly. Instead, the discretised u-momentum (3) reads:

$$\frac{u^{n+\frac{1}{2},p+1}-u^{n}}{\frac{1}{2}\Delta t}+u^{n+\frac{1}{2},p+1}D_x^{2^{nd}\,cntrl}\left\{u^{n}\right\}+v^{n+\frac{1}{2}}D_y^{2^{nd}\,cntrl}\left\{u^{n}\right\}+g\frac{h^{n+\frac{1}{2},p}}{h^{n+\frac{1}{2},p+1}}D_x^{2^{nd}\,cntrl}\left\{\zeta^{n+\frac{1}{2},p+1}\right\}=0. \tag{3}$$

Using (3), the new iterate $h^{n+\frac{1}{2},p+1}u^{n+\frac{1}{2},p+1}$, with iteration level p, is expressed into old-time level variables as well as into $\zeta^{n+\frac{1}{2},p+1}$ and subsequently substituted into the following discretised conservation equation:

$$\frac{\zeta^{n+\frac{1}{2},p+1}-\zeta^{n}}{\frac{1}{2}\Delta t}+D_x^{2^{nd}\,cntrl}\left\{h^{n+\frac{1}{2},p+1}u^{n+\frac{1}{2},p+1}\right\}+D_y^{2^{nd}\,cntrl}\left\{h^{n}v^{n}\right\}=0, \tag{4}$$

with h centrally-averaged to (u,v) points yielding a tri-diagonal system in x-direction that is solved by the Thomas algorithm and subsequently iterated on (p) to convergence. Note that the ratio $h^{n+\frac{1}{2},p}/h^{n+\frac{1}{2},p+1}$ in the last term of (3) ensures mass-conservation at every p-iteration. In the subsequent half-time step, the u-momentum equation is formulated and solved as (2) and then the inviscid momentum (3) for v is coupled to (4) while (3) is formulated implicitly in v-component and in y-direction.
For the full time step, the coupled advection-conservation schemes are second-order in time with fourth-order dissipation in space and unconditionally stable (Stelling, 1984). The viscous force is integrated explicitly, invoking a mild time step limitation.

For DNS or LES applications, a disputable disadvantage is that the cyclic combination of 2nd-order upwind and 2nd-order central advection in (2-4) are neither strictly momentum nor strictly energy conserving. On the other hand, however, the tendency of creating velocity wiggles in inviscid simulations using the energy-conserving scheme of Arakawa & Lamb (1981) appear to invoke more dissipation in simulations when viscous stresses are included (Hólm, 1995). Further, the semi-implicit coupling of the pressure $g\zeta$ to the momentum equations (2-3) as well as to the conservation equation (4) tends to conserve the energy stored in the free-surface or compressible velocity modes induced by the velocity-advection operator. Depending on the flow and on the advection scheme, the latter may convert incompressible energy modes into compressible energy modes that are subsequently removed/dissipated by pressure

correction/projection schemes that are customary in fixed-volume incompressible DNS/LES solvers.
This section is concluded by introducing the time-step limitations based on accuracy, rather than stability, of advection and of the long-wave or barotropic (BT) velocity modes on a square mesh with grid size Δx:

$$\Delta t_A = \sigma_A \frac{\Delta x}{\max(|\underline{u}|)}; \Delta t_{BT} = \frac{\sigma_{BT}}{2\sqrt{2}} \frac{\Delta x}{\sqrt{gh}} \rightarrow \frac{\Delta t_A}{\Delta t_{BT}} = 2\sqrt{2} \frac{\sigma_A}{\sigma_{BT}} \frac{\sqrt{gh}}{\max(|\underline{u}|)}. \tag{5}$$

The first criterion originates from the semi-implicit x-advection term in (3) and it demands $\sigma_A<4$ (Stelling, 1984, p. 165). Benqué et al., (1982) proposed the second criterion with $\sigma_{BT}<4\sqrt{2}$ for avoiding aliasing in wave propagation using ADI and staggered grids e.g. over bed topography. For the temporal representation of advected and deforming vortices we believe $\sigma_A<O(0.3)$ would be a proper *space-time consistency criterion.* For Froude numbers $U / g\sqrt{h} > O(0.15)$, using the limitation $\sigma_{BT} < 4\sqrt{2}$, the latter criterion coincides, i.e. $\Delta t_A \approx \Delta t_{BT}$. However, smaller Froude numbers are typical for our applications and then the accuracy of simulating BT modes limits the time step.

3. Some considerations of 2D turbulence with a free surface

For an overview of properties of 2D turbulence, such as the inverse energy cascade related to vortex merging, we refer to e.g. (Lesieur, 1997). For an closed basin with water volume V, this section considers briefly the possible coupling of 2D turbulence (vortical) motions to free-surface (BT) motions. The frictionless SWE (1) then yields the following conservation property (Arakawa & Lamb, 1981):

$$\frac{\partial}{\partial t} \iint h\left\{\tfrac{1}{2}\underline{u}\cdot\underline{u} + \tfrac{1}{2}gh - gd\right\} dx dy = 0, \tag{6}$$

where the first term represents the kinetic energy (KE) and the sum of second and third term the potential energy (PE). For a closed basin with horizontal bed (constant d), the third term cancels due to mass conservation. In addition, from the frictionless SWE (1) also follows

$$\frac{D^2\zeta}{Dt^2} - gh\nabla^2\zeta = h\left\{D_{ij}D_{ij} - \omega_z^2\right\} + h\left\{\frac{1}{h}\frac{D\zeta}{Dt}\right\}^2; \frac{D\zeta}{Dt} = \frac{\partial}{\partial t} + \underline{u}\cdot\nabla, \tag{7}$$

with horizontal-strain rate tensor D_{ij} based on $\underline{u}$ and vertical vorticity component ω_z. From the frictionless SWE also follows the conservation of potential vorticity (PV) ω_z / h:

$$\frac{D}{Dt}\left(\frac{\omega_z}{h}\right)=0. \tag{8}$$

A priori (6-8) suggest that 2D turbulence in free-surface flows differs from 2D turbulence in rigid fluid volumes. For example, the LHS of (7) represents the long-wave propagation of a surface perturbation ζ associated with PE in (6) whereas (6) shows that PE is reversibly exchanged with KE. Further, the RHS of (7) acts as source of surface perturbations ζ of which the vertical vorticity obeys (8). Note that (7) is similar to Lighthill's equation for sound generation by turbulence. The RHS of (7) equals the Weiss-function, see e.g. (Basdevant & Philipovitch, 1994), where the last term is due to the vertical strain rate in long waves.

We conclude that *a priori* deviations may exist between the evolution of 2D turbulence simulated with a rigid lid, such as by Clercx et al. (1999), or with the SWE (1). Nevertheless, detailed analysis (Vossen, 2000) of our SWE simulations as well as animations of vorticity combined with surface elevation show that (7) can be approximated well by the rigid-lid counterpart with pressure $g\zeta$:

$$\nabla^2(g\zeta)=\omega_z^2-D_{ij}D_{ij}. \tag{9}$$

4 Numerical initialisation of 2D turbulence in a free-surface fluid

Clercx et al. (1999) solve the viscous 2D stream function and vorticity equations using 288^2 Chebyshev polynomial expansion and they initiate 2D turbulence by random 64^2 Chebyshev modes that in general do not obey incompressibility. The laboratory experiments of Tabeling et al. (1991) start with 2D chessboard vortices. In both cases, our simulations initiated with a spatially constant ζ show that much PE is generated as freely-propagating waves, see LHS of (7). For a proper comparison with experiments we must initiate the velocity-surface field more carefully as follows. Define, at t=0, the master velocity field as $\underline{u}_0$ either based on 64^2 Chebyshev modes or chessboard vortices. Next, the associated incompressible field $\underline{u}(\underline{x},0)$ is derived from:

$$\underline{u}(\underline{x},0)=\underline{u}_0+\nabla\lambda \text{ with } \nabla^2\lambda=-\nabla\cdot\underline{u}_0, \tag{10}$$

with $\nabla\lambda$ the corrected velocity field such that $\nabla \cdot \underline{u}(\underline{x},0)=0$ holds on the computational grid. For closed boundaries (10) yields less KE in $\underline{u}(\underline{x},0)$ than in $\underline{u}_0$. Likewise, Clercx et al. (1999) report a decrease in KE at their first time step that yields $\nabla \cdot \underline{u}(\underline{x},\Delta t)=0$. With $\underline{u}(\underline{x},0)$ by (10), the initial surface elevation $\underline{\zeta}(\underline{x},0)$ is obtained from (9) as the quasi-steady approximation to (7). Following this initialisation, our SWE simulations then evolve gradually in time and space without notable wave-like motions.

5. Investigation and estimation of numerical dissipation

In view of (5), the appropriate time step was investigated by inviscid simulations of (1) initialised by Clercx's random 64^2 Chebyshev modes and the procedure given in section 4. Figure 1 presents the temporal evolution of volume-integrated KE in a basin of width W=1m with 1 cm still-water depth and $|u'|$=4 mm/s using 100^2 square grid. In all cases, $\sigma_A \leq 0.24$ holds but Figure 1 shows that only if $\sigma_{BT} < 4\sqrt{2}$ is satisfied then near conservation of KE is obtained. Therefore, $\sigma_{BT} < 4\sqrt{2}$ is applied in all subsequent simulations.

For practical reasons we estimate a numerical viscosity ν_{num}, equivalent to the kinematic viscosity, by

$$\nu_{num} = -\frac{1}{2\Theta}\frac{\partial E_k}{\partial t} \text{ with } E_k = \tfrac{1}{2}\rho\iint h\left(u^2+v^2\right)dxdy \text{ and } \Theta = \tfrac{1}{2}\rho\iint h\omega_z^2\,dxdy, \quad (11)$$

although the advection operators yield 4th order dissipation. Series of inviscid runs with variations of grids N_p*N_p (N_p= 50, 100, 200, 500), of basin size (1-100m) and initial fields with random Chebyshev polynomials or chessboard vortices (1, 4, 16 and 100) yield the following approximation:

$$\nu_{num} \approx \frac{|u'|\Delta x}{8\sqrt{N_p}} \quad ; \quad N_p = \frac{W}{\Delta x} \quad , \quad (12)$$

with N_p proportional to the resolved band width. Despite the strong temporal merging of vortices (see figure 5), Figure 2 presents an example of the marginal temporal dependence of ν_{num} estimated through (11) and thus suggests its validity as estimator for numerical dissipation.

6. Simulations of 2D turbulence in free-surface experiments

The upper part of figure 5 presents particle tracks observed in a 1*1 m^2 reservoir (Maassen, 2000). Although the top layer floats on a denser salt-water layer, Maassen (2000) notes a significant interfacial friction reducing the effective Reynolds number by a factor 5. The lower part of figure 5 presents the vorticity contours simulated by the shallow-water solver but without interfacial friction. The evolution of vorticity patterns is similated qualitatively well by our shallow-water solver. Due to the uncertainty in modelling the interfacial friction, i.e. c_f in (1), we prefer the comparison with simulations by Clercx et al. (1999) who applied a solver dedicated to this type of experiments.

For Reynolds number Re=2000, Clercx et al. (1999) simulated decaying viscous 2D turbulence with no-slip wall conditions but without bed or interfacial friction. They define Re and the temporal scale T by

$$\mathrm{Re} = \frac{\frac{1}{2}W|u'|}{\nu} \quad ; \quad T = \frac{\frac{1}{2}W}{|u'|} \quad ; \quad \tfrac{1}{2}\Delta y^{+} \approx \frac{\mathrm{Re}}{17N_p} \quad , \tag{13}$$

with W the width of the square basin. For resolving viscous boundary layers with a square grid the last expression in (13) should equal unity and this expression determines that N_p=200 is adequate for a 2D DNS with our shallow-water solver. Figure 3 includes the simulations of Clercx et al. (1999) solved by 288^2 Chebyshev modes and we applied their initial velocity field based on 64^2 Chebyshev polynomials but corrected to an incompressible flow through (10).

Figure 3 presents the relative decay of volume-integrated KE as well as volume-integrated enstrophy, as defined by (11), against time scaled by T defined in (13). Under these conditions, the overall numerical viscosity (12) of the shallow-water solver is estimated to be about 0.2ν. Nevertheless the decay simulated with the shallow-water solver is comparable or even less than simulated by Clercx et al. (1999).

7. Conclusions and discussion

We conclude that the general-purpose shallow-water solver Delft3D-Flow is capable of simulating vortex merging and the decay of 2D turbulence in a viscous fluid without notable numerical diffusion (figure 3). From a simulation point-of-view, the most notable aspect of the free surface in 2D turbulence reads as follows. Animations of vorticity and surface elevations show that most of the free-surface elevations are induced by the Weiss function, RHS in (9). Despite that the free-surface elevations carry marginal available potential energy, compared to kinetic energy, their evolution must be carefully simulated else kinetic energy is generated artificially (Figure 1). The latter demands for the barotropic Courant number $\sigma_{BT} / 4\sqrt{2} \leq 1$ (figure 1) and it is very restrictive compared to other accuracy and stability conditions for the shallow-water solver

Delft3D-Flow. The reason for the constraint on this typical wave-propagation condition is not clear. We speculate that the Poisson equation (9) is essential and needs to be solved accurately. In SWE, however, the solution of (9) is obtained through (7) and, if σ_{BT} is too large, errors in the rapid propagation of surface perturbations spoil the approximation to (9).

8. Acknowledgments

We appreciated the stimulating discussions with Dr. Clercx and Prof. Van Heijst (Eindhoven University of Technology) as well the patient support of our colleague Dick Verploegh in post-processing the simulation.

References

1. Arakawa, A. & V.R. Lamb 1981 A potential enstrophy and energy conserving scheme for the shallow-water equations. *Monthly Weather Rev.*, vol. 109, pp. 18-36.
2. Basdevant, C. & T. Philipovitch 1994 On the validity of the "Weiss criterion" in two-dimensional turbulence. *Physica D,* 73, pp. 17-30.
3. Benqué, J.P. J.A. Cunge, J. Feuillet, A. Hauguel & F.M. Holly 1982 New method for tidal current computation. *J. Waterway, Port, Coastal and Ocean Div. ASCE,* 73, pp. 396-417.
4. Clercx, H.J.H., S.R. Maasen & G.J.F. van Heijst 1999 Decaying two-dimensional turbulence in square containers with no-slip or stress free boundary conditions. Phys. Of Fluids, vol. 11, no. 3, pp. 611-626.
5. Hólm, E.V. 1996 Energy and enstrophy conservation properties of high-order non-oscillatory advection schemes. *Tellus*, 48A, pp. 122-137.
6. Kernkamp, H.W.J. & R.E. Uittenbogaard 2001 2D-LES of a free-surface mixing layer. *Proc. Direct and Large-Eddy Simulation Workshop 4,* (ed's B.J. Geurts, F. Friedrich & O. Metais), Enschede, The Netherlands, July, pp. 213-216.
7. Lesieur, M. *Turbulence in fluids.* Kluwer, Dordrecht, The Netherlands.
8. Maassen, S.R. 2000 *Self-organisation of confined two-dimensional flows.* Ph.D. Thesis, Eindhoven University of Technology, August.
9. Stelling, G.S. 1984 *On the construction of computational methods for shallow water flow problems.* Rijkswaterstaat communications, No. 35.
10. Tabeling, P., S. Burkhart, O. Cardoso & H. Willaime 1991 Experimental study of freely-decaying two-dimensional turbulence. *Phys. Rev. Letters*, vol. 67, no. 27, pp. 3772-3775.
11. Vossen, van, B. 2000 *Horizontal Large Eddy Simulations; evaluation of flow computations with Delft3D-Flow.* M.Sc.Thesis Delft University of Technology, MEAH-197, Aug.

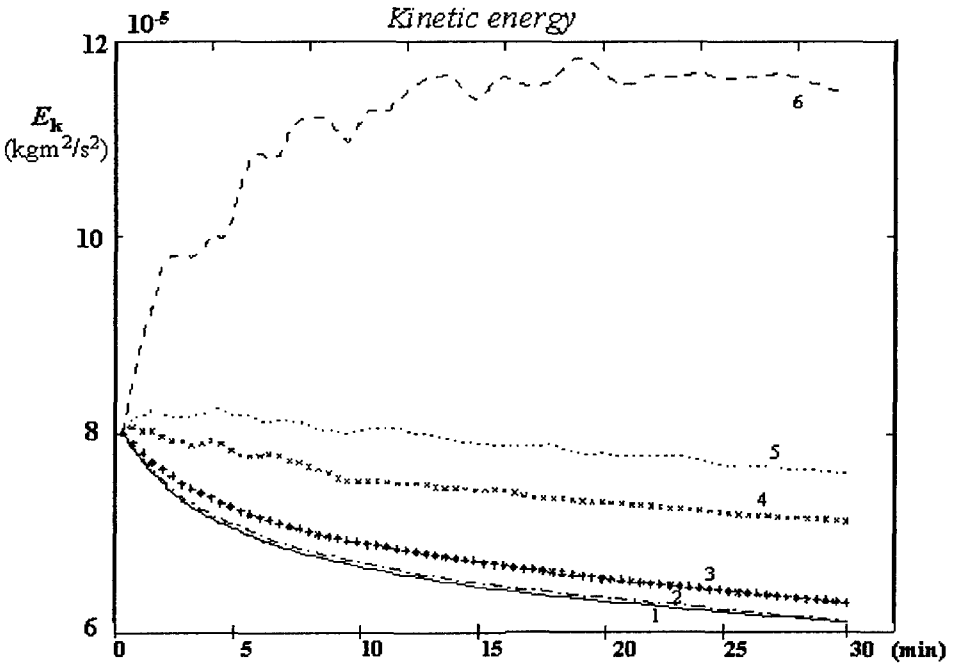

Figure 1. Decay of kinetic energy 100^2 grid, 1*1*0.01 m^3, |u'|=4 mm/s, initial random field, for $\sigma_{BT} / 4\sqrt{2}$ = 9.4 (6) ; 4.8 (5) ; 3.9 (4) ; 1.9 (3) ; 0.94 (2) ; 0.47 (1).

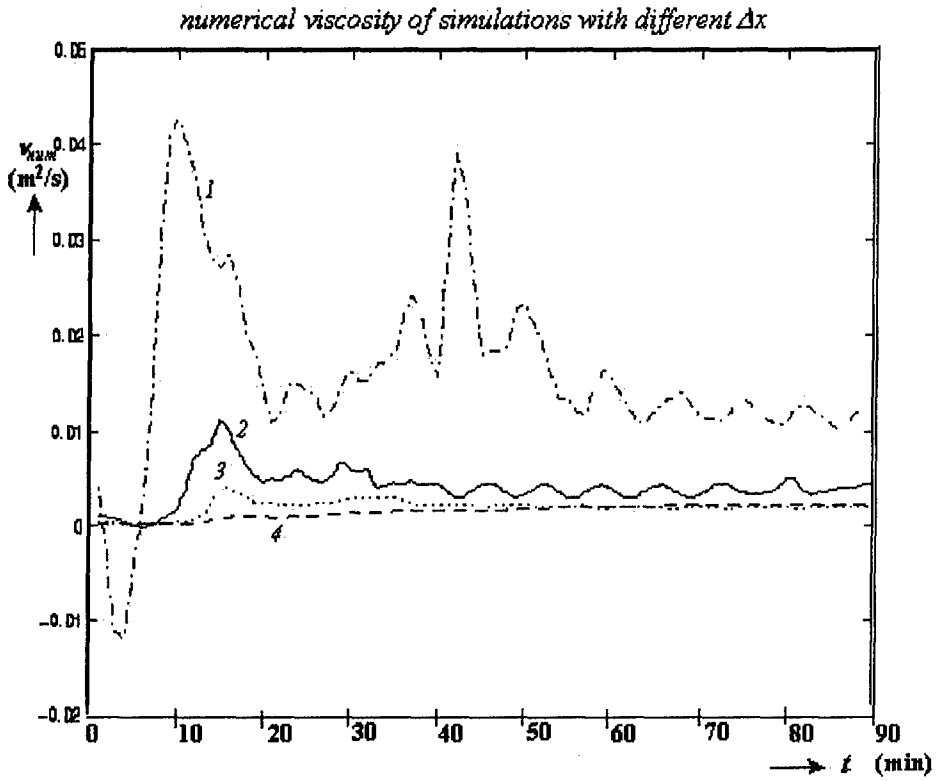

Figure 2. Numerical viscosity, estimated by (11), for 50×50 (1), 100×100 (2), 200×200 (3) and 500×500 (4) grid cells ; 100*100*1 m^3 ; |u'|=0.4 m/s, initialized by 16 chessboard vortices.

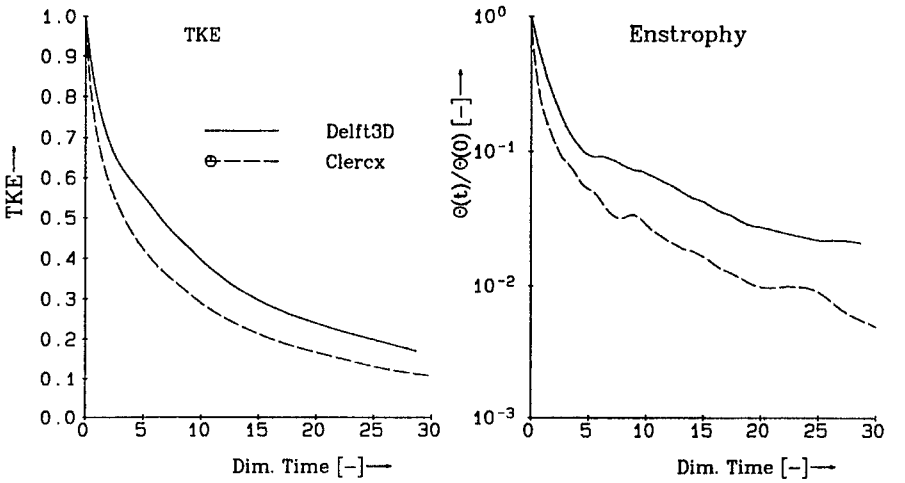

Figure 3. Relative decay of volume-integrated kinetic energy and enstrophy, see (11) of 2D turbulence initiated by a random field at Re=2000 and T=125 s time scale. Comparison between the shallow-water solver (Delft3D) using 200^2 square grid at σ_Λ=0.012 and $\sigma_{BT}/4\sqrt{2}$ =0.47, see (5), with simulations in (Clercx et al., 1999).

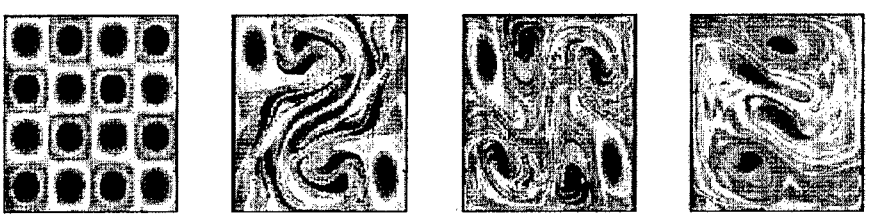

Figure 4. From left to right t= 0 ; 15 ; 20 ; 30 minutes. Evolution of 4*4 chessboard vortices on a 500^2 grid of 100*100*1m^3 ; |u'|=0.4 m/s ; inviscid shallow-water simulation.

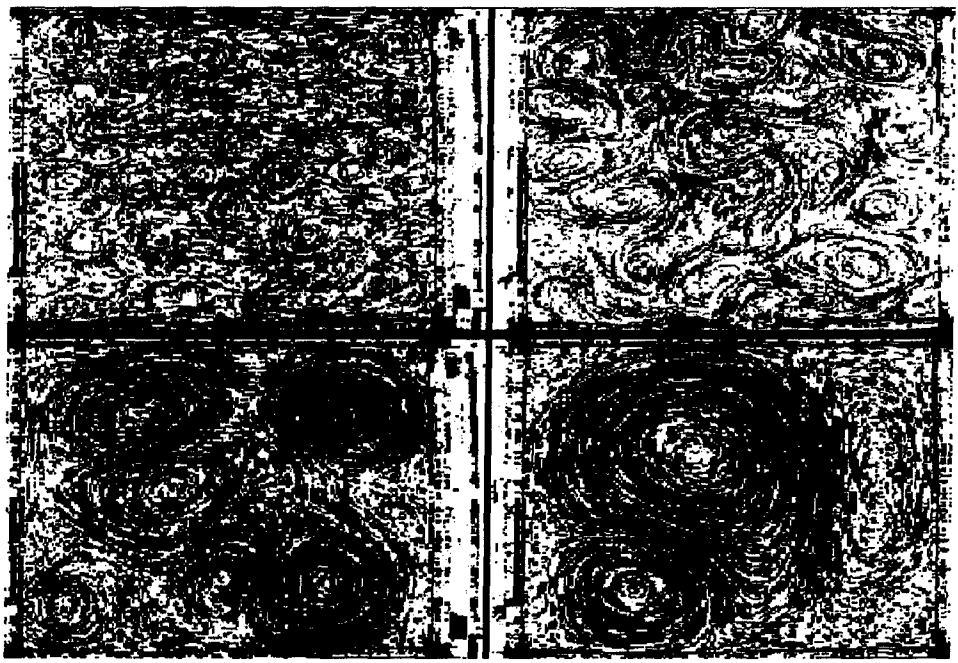

Figure 5. Particle tracks in the free-surface water layer on top of a dense salt layer 10 seconds (up-left), 1 minute (up-right), 5 minutes (down-left) and 50 minutes after passage of a raKE (Maassen, 2000). Below, iso-contours of vertical vorticity, simulated by Delft3D for conditions of figure 3 and similar to observations above.